



Removal of suspended matter and salts on ultrafiltration cellulose acetate/expanded polystyrene waste grafted PEG composite membrane

Mahmoud Fathy^a, Hager R. Ali^a, Yasser M. Moustafa^a, Abeer El Shahawy^{b,*}

^a*Petroleum Research Institute (EPRI), 1 Ahmed El-Zomer St., Nasr City, 11727 Cairo, Egypt, emails: fathy8753@yahoo.com (M. Fathy), d_hager80@yahoo.com (H.R. Ali), Ymoustafa12@yahoo.com (Y.M. Moustafa)*

^b*Department of Civil Engineering, Faculty of Engineering, Suez Canal University, P.O. Box: 41522, Ismailia, Egypt, email: abeer_shahawi@eng.suez.edu.eg (A. El Shahawy)*

Received 25 September 2019; Accepted 13 April 2020

ABSTRACT

Ultrafiltration (UF) cellulose acetate (CA)/expanded polystyrene (PS) waste grafted polyethylene glycol (PEG) composite membrane UF was prepared using CA mixed with waste PS and grafted with PEG by casting polymerization. In the present study, suspended organic matters (kaolin) were used in the sizes of micro-particles (0.2–0.4 μm) like organic foulants particulates in secondary wastewater, respectively. X-ray diffraction (XRD), transmission electron microscopy, Raman, and Fourier-transform infrared spectroscopy were used in this study. The scanning electron microscopy images exhibited a uniform and dense structure for the membranes. The amorphous structure membranes were detected through the XRD pattern. Solutions of (CaCl, MgCl, NaCl, KCl, Na₂CO₃) and kaolinite as suspension solids were used for membrane selection and permeability under the effects of pH, applied pressure, and kaolinite and ions concentration. This study was undertaken to evaluate the performance of the water recovery system for the CA/PSPEG to assess its self-sustainability. Consequently, the membrane (CA/PSPEG) displays excellent overall completion in separation performance compared with pure PS membranes. The modified membranes achieved a 99% rejection in comparison to 90% for the basic membrane. This membrane could be an exceptional material for water treatment purposes.

Keywords: Membrane; Ultrafiltration; Polystyrene; Kaolin; Performance; Foulants

1. Introduction

In recent decades, membrane separation processes have been extensively used in different applications including gas separation [1], water treatment [2], pharmaceutical processing, food industries [3], etc. Additionally, drinking water scarcity issues have attracted growing attention by the research community and thus various kinds of membrane technologies have been applied for water treatment (membrane separation and purification). Ultrafiltration (UF) is one of the promising membrane technologies in

terms of efficiency and energy-saving. It is widely used in several fields such as water purification, food and dairy industries, oil-water separation, protein purification, wastewater treatment, separation and purification in the textile, and as a pretreatment stage in the nanofiltration (NF) and reverse osmosis membranes systems [4]. Electrospun nanofibers are attractive materials for UF due to their morphology, which can be controlled through their processing parameters and thus their surface can be altered by various means to get different functions [5]. Recently, Luo et al. [6] studied the effect of supersonically

* Corresponding author.

blown ultrafine nanofibers (20–50 nm) on top of the electro-spun layer. It was found that the filtration efficiency increased for particles (<200 nm) which was attributed to the increased diffusion of the nanoparticles through Van der Waals attraction [7].

Many electrospun polymers have been considered for liquid filtration including nylon 6, polyethersulfone (PES), polyacrylonitrile, polyvinylidene fluoride, and polyvinyl alcohol. Despite the diversity of materials, there are still several challenging issues that were highlighted by Zhu et al. [7] and Lim et al. [8]. For example, enhancing the mechanical strength of the membrane sufficiently to achieve high permeate flux and controlling the microstructure of the polymeric membranes have been considered challenging factors in chemical separation, and thermal desalination using membrane distillation [9]. Recently, the incorporation of aromatic polymers into natural polymeric matrices for the sake of preparation of advanced membranes with enhanced properties has been widely reported in the literature [10,11]. Polystyrene (PS) fillers are introduced into cellulose acetate (CA) matrix to synthesize porous composite membranes with an improved thermal and mechanical performance for desalination and water treatment [12,13]. The chemical recognition of the analyte ion, F , is based on the partition of the hydrophilic ion from the aqueous sample into the lipophilic membrane phase [14]. The partition coefficient of the ion used to describe this partition, k_p , is affected by the dielectric constant of the medium, and the size and charge of the analyte ion. The increase in the ion size and the decrease in the ion charge caused the increase of the ion partition in the lipophilic membrane [15].

The general scope of the present work is to reuse the waste polymer in membranes-based water treatment and desalination to increase the water production rate and reduce the treatment cost. CA is a natural polymer that is promising in water treatment but bacteria can destroy its skeleton and deteriorate the performance in a short time. Accordingly, the current work attempts to improve its efficiency by PS waste polymer that can withstand bacteria action for a long time and thus can result in high permeate flux. The performance of the membrane was tested using binary solutions of CaCl₂, MgCl₂, NaCl, KCl, Na₂CO₃, and kaolinite as suspension solids.

Additionally, the effect of feed pH and kaolinite fouling in a CA/PSPEG process was investigated with different concentrations of kaolinite.

2. Materials and experimental

2.1. Materials

Styrofoam (grade S-7054; density, 490 g L⁻¹) supplied by BIPC, Egypt, and polyethylene glycol 400 (PEG 400), supplied by Sigma-Aldrich, USA were used in the membrane fabrication. Dimethylformamide (DMF), acetone, chloroform solvent was supplied by Merck Inc., Germany, was also used as solvent and functional groups agent, respectively. Kaolinite is one of the most common minerals; it is mined, as kaolin, in Egypt – South of Sinai – sizes of 0.2–0.4 μm. Distilled water was used during the experimental work. All soluble salts along with reagents used in the experiments were of analytical grade and obtained from Sigma-Aldrich

2.2. Membrane characterization

2.2.1. Morphological studies

The membrane performance is influenced significantly by the membrane structure, especially the spatial distribution of the ionic site. Scanning optical microscopy (SOM, Olympus, Model IX 70, in transmission mode) and scanning electron microscopy (SEM) were used for examination of the prepared membranes structures. In SOM analysis, small pieces of the prepared samples were organized and mounted between lamellas then inspected by the optical microscope. For the SEM analysis, the membranes were frozen in liquid nitrogen, fractured, and sputtered with gold then observation was undertaken using the electron microscope.

2.2.2. X-ray diffraction

For microstructural studies of the prepared composite membranes, X-ray diffraction (XRD) patterns were carried out by an X-ray diffractometer (XRD, model X'Pert Pw 3373, $k_{\alpha} = 1.54 \text{ \AA}$, Philips, Holland).

2.2.3. Fourier-transform infrared spectroscopy

Fourier-transform infrared spectroscopy (FTIR) was performed using a Bruker Vector 33 spectrometer with KBr pellets (Egypt). The reflectance spectra were accumulated over the wave range 400–4,000 cm⁻¹ at a spectral resolution of 4 cm⁻¹ with scans of 32.

2.2.4. Raman analysis

Raman spectra were taken using HORIBA Jobin Yvon LabRAM, (Darmstadt, Germany) with 514 nm laser excitation from argon-ion laser and a grating of 1,800 cm⁻¹ was used to record the spectra.

2.2.5. Zeta optional

300 mL of 0.196 wt.% nanocellulose water suspension was prepared and its zeta potential value at different pH (3–10) was measured at 25°C using the Zeta Probe Analyzer (Colloidal Dynamics Inc., Ponte Vedra Beach, FL, USA). 0.1 M NaOH and HCl solutions were used for pH adjustment.

2.3. Synthesis of the composite membrane

Porous UF membranes based on Styrofoam (grade S-7054; density, 490 g L⁻¹) and PEG (up to 20 wt.%) composites were prepared from the 12 wt.% solutions in dimethylacetamide (DMA). The membranes were obtained cast using the immersion precipitation in the distilled water bath at 25°C [16]. After the film formation, the membranes were left for 12 h in distilled water. The casting solution contained 20% maximum content of [Pluronic F127 (F127, MWn: 12,600 Da) was purchased from Sigma-Aldrich, USA] because a further increase of its concentration led to the inability to operate the membrane under pressure (low mechanical strength).

2.4. Commercial membranes solute filtration test

CA/PSPEG membrane was used in the solute filtration test for the molecular weight cutoff (MWCO) study. MWCO

of all membranes were determined by using PEG with molecular weight (MW) ranges from 600 to 20,000 g mol⁻¹. The solute MW ranges were divided into two categories (i) NF range for MWCO below 2,000 g mol⁻¹ and (ii) UF range for MWCO above 2,000 g mol⁻¹. Table 2 and Fig. 4 show the results of the fluxes and MWCO for CA/PSPEG membranes tested by both methods. It was found that the fluxes for the membranes in water were higher than in the PEG solutions, as expected. This is because the solutes in the solution hinder the permeation of water thus reducing the flux. The PEGs used for the flux in PEGs are from PEG 600 to PEG 20000. This flux value was averaged out from the flux obtained at each PEG solution used. The higher the MW of PEG used, the lower the flux recorded.

2.5. Experimental setup and operational conditions

Fig. 1 depicts the UF membrane pilot plant which is comprised of 90 L tank connected in series with 30 L permeate tank. The membranes used in the UF process were (CA/PSPEG) membranes with a pore size of 0.04 μm and a permeation area of 70 m².

2.6. Filtration and membrane fouling tests

The filterability of the colloidal clay water was assessed by membrane fouling index (MFI), which was determined in dead-end filtration batch tests. The MFI provides an idea of the fouling potential of the colloidal clay water [17]. A higher MFI value can result in higher performance in UF systems. The filtration batch tests were conducted under unstirred conditions, using a flat sheet membrane with a nominal pore size of 0.2 μm [8,18]. All experiments were carried out at 0.3 bar pressure, using a new flat sheet

membrane for each test. The permeation flux was obtained by weighing the cumulative permeate using an electronic balance. The filtration experiments were carried out using the water suspended solids and also a supernatant solution. Such procedure was followed to separately evaluate the filterability of all colloidal clay water and that of its colloidal and dissolved components. The slope of the linear region of the turbidity vs. time (*t*) curve represents the MFI values. [19].

2.7. Operating procedure for kaolinite removal

The binary and ternary solutions were performed to study the separation capability of the CA/PSPEG membrane. Firstly, the effect of temperature and kaolinite feed concentration was studied at natural pH 6.50. The applied pressure and the feed concentration ranged from 2 to 6 bar and 25 to 100 mg L⁻¹ of kaolinite, respectively. The effect of the pH of the feed stream on the membrane rejection was also investigated in the pH range of 3–12 for feed concentration of 50 mg kaolinite L⁻¹ at a pressure of 6 bar. The acidity and alkalinity were adjusted by the addition of HCl or NaOH solutions with a concentration of 1 M. Finally, kaolinite suspension solution filtration was examined at different time intervals at natural pH 5.70–6.50 for contact time evaluation studies [20]. The range of 1, 5, and 10 mg kaolinite L⁻¹ of the total kaolinite concentration were prepared and studied [21].

2.8. Effect of co-excising ions on the kaolinite removal

Firstly, the effect of applied pressure and salts feed concentration was examined for monovalent cations NaCl and

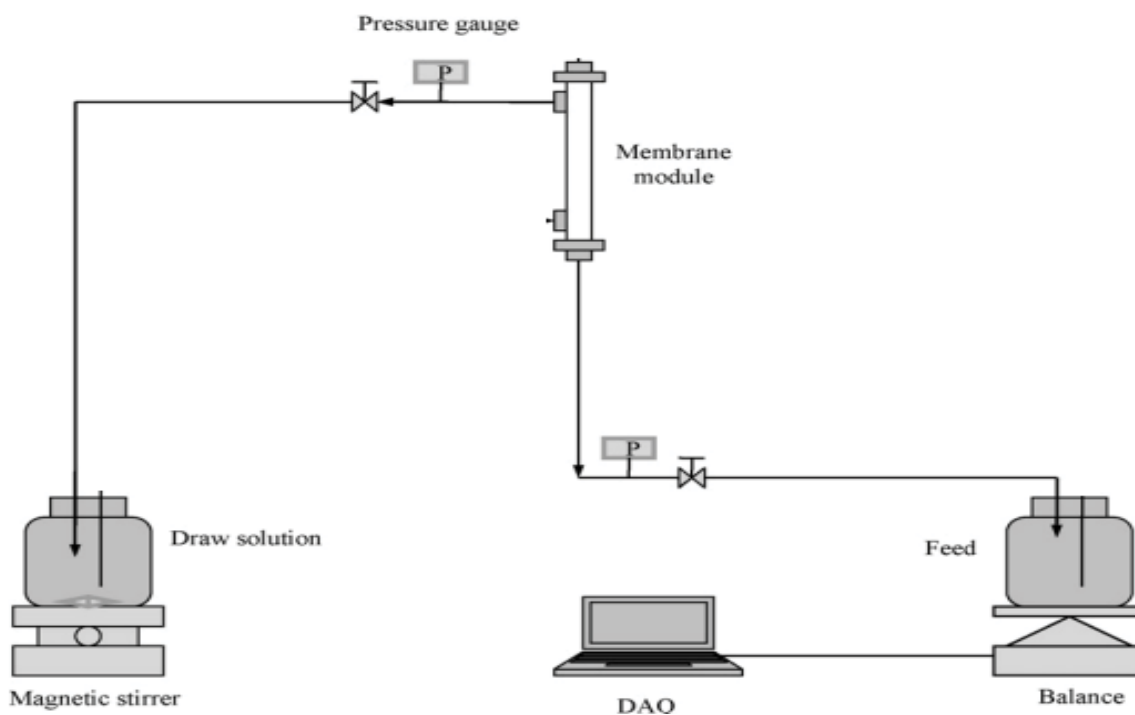


Fig. 1. UF membrane schematic flowchart.

KCl and divalent cations CaCl_2 and MgCl_2 at natural pH varied from 5.70 to 6.50. The applied pressure was varied from 2 to 6 bar and the feed concentration was in the range of 25–100 mg L^{-1} of salts. The effect of the pH value of the feed stream on the membrane rejection was also investigated in the pH range 3–9 for feed concentration of 50 mg salts L^{-1} at a pressure of 6 bar. The pH value was adjusted by the addition of HCl or NaOH solutions with a concentration of 1 M [22].

Secondly, the filtration of salts solutions containing monovalent cations NaCl and KCl and divalent cations CaCl_2 and MgCl_2 as well as monovalent and divalent cations NaCl and CaCl_2 were studied at different applied pressure at natural pH 5.70–6.50. The total concentration of salts ions in the prepared solutions was studied over the range of 25–100 mg salts L^{-1} [23].

The filtration experiment was implemented at an applied pressure of 2, 4, and 6 bar at natural pH and concentration of 50 mg salts L^{-1} . The effect of pH on salts rejection was examined between pH 3 and pH 9 for the different ternary solutions (with a total concentration of 50 mg salts L^{-1} and a pressure of 6 bar) [24].

The third step involved the study of three commercial mineral water at a pressure of 6 bar and natural pH (pH 7.00). Before filtration, an amount of nitrate salt equivalent to 25 $\text{mg NO}_3/\text{L}$ was added to water samples using two NO_3^- sources NaNO_3 and $\text{Ca(NO}_3)_2$ [25].

3. Results and discussion

3.1. FTIR analysis

The FTIR spectra of the PES and PES/CA membrane modified with PEG were compared to observe the vibrational

pattern changes as displayed in Table 1. Fig. 2 depicts that, for the PS, the weak peak occurs at $1,500\text{cm}^{-1}$, which specified the presence of C–O–C [26]. The C=O were located at $1,739.79\text{ cm}^{-1}$ in the stretching modes [17,18,20]. The band obtained at 902.69 cm^{-1} was attributed to a pyranose ring present in CA [16]. For the FTIR spectrum of the blend membrane with PEG 600 (Fig. 1), The –OH band broadness decreases in the region from $3,200\text{--}3,500\text{ cm}^{-1}$. The aldehyde carbonyl group in the CA ring existed in the band at $1,740\text{ cm}^{-1}$.

Fig. 3 shows the spectrum of the PES and PES/CA membrane modified with P. The characteristics Raman signals can be observed at $3,444$ and $1,678\text{ cm}^{-1}$ matching the oxygen–hydrogen bond vibration and carbonyl group (C=O) vibration present in the carboxylic groups. The carbon–carbon double bond (C=C) appears at $1,654\text{ cm}^{-1}$ with the stretching vibrations while the in-plane bending of the

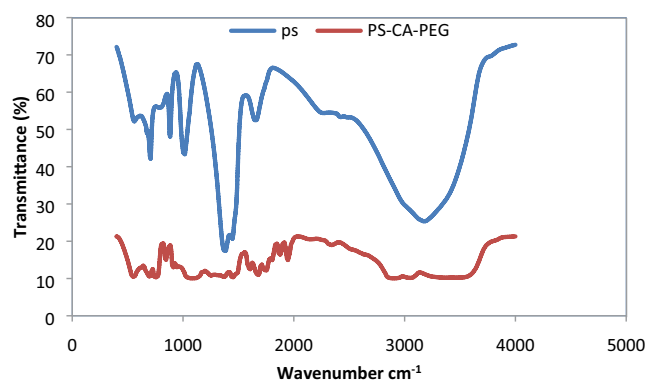


Fig. 2. FTIR of PS and PS-CA-PEG composite membranes.

Table 1

Surface functional groups observed one of the PES and PES/cellulose acetate membrane modified with polyethylene glycol were compared to observe the vibrational pattern changes using FTIR

Band position (cm^{-1})	Functional groups
PS	
Strongest peak at $1,035\text{ cm}^{-1}$	C–O–C [22]
Stretching modes at $1,739.79\text{ cm}^{-1}$	C=O [17,18,20]
Band at 902.69 cm^{-1}	Pyranose ring in cellulose acetate [16]
Blend membrane with PEG 600	
Region from $3,200\text{--}3,500\text{ cm}^{-1}$	OH band broadness decreases
Band at $1,740\text{ cm}^{-1}$	Aldehyde carbonyl group in the CA ring
Band at $1,447\text{ cm}^{-1}$	Stretching modes of the C=C double bond
Characteristic peak at around 685 cm^{-1}	Out-of-plane bending of C–H vibration
Existence of a band at $1,740\text{ cm}^{-1}$	Formation of new hydrogen bonds between O–H groups of CA and the C=O groups of PEG 600. The presence of such O–H–C=O interaction implied an excellent miscibility of CA and PEG 600 in the blend membranes
Blend at $2,873.94$.	Band shift in C–H stretching occurs due to hydrogen bonding between CA and PEG 600
Blend for C–O bands at $1,232.51$.	Band shift with broadening
Stretching band is in blended bands	Small decrease in intensity of C–H
Small bands at 830.93	Validate the presence of PEG 600 in blend [19]
Spectra of the blend membranes, broad band around at $1,688\text{--}1,681\text{ cm}^{-1}$	Stretching vibration of C=N due to the presence of a DMF ring

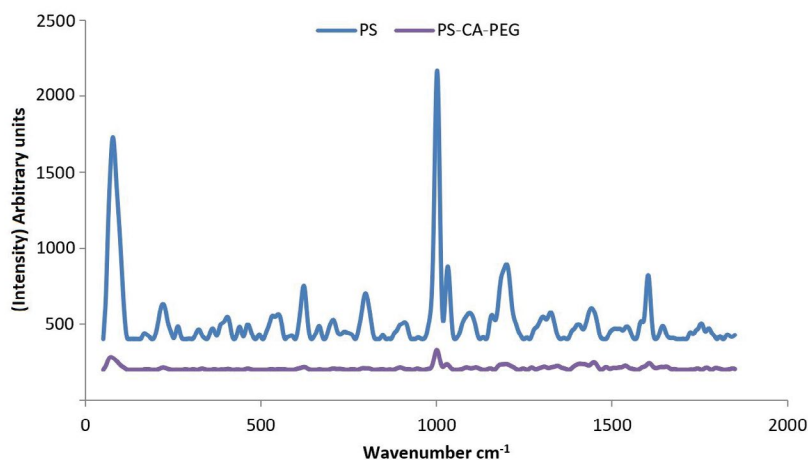


Fig. 3. Raman spectroscopy for PS and PS-CA-PEG membranes.

O–H bond can be placed at $1,496\text{ cm}^{-1}$. The bands at $1,306$; $1,224$; and 905 cm^{-1} correspond to C–O bond vibrations. The peak at $1,224\text{ cm}^{-1}$ had a contribution from the C–C bonds. The pyranose ring signal was detected at $1,081\text{ cm}^{-1}$ and the characteristic Raman signals for acetyl group at $1,731$ corresponding to the vibration of the carbonyl group (C=O) during mixing the polymer.

3.2. SEM and XRD analysis

Fig. 4 depicts the cross-sectional SEM images of unmodified and CA/PSPEG composite membranes. The SEM images showed a uniform and dense structure for the prepared membranes. The XRD was used to inspect the membrane structures. As shown in Fig. 4, there is no peak in the XRD pattern for the virgin membrane and the modified polyvinylchloride/carboxymethyl cellulose. The results demonstrated an amorphous structure for the prepared membranes [18].

Fig. 4 demonstrates also the morphology of the asymmetric composite membrane cross-section as observed with the SEM. The membrane is composed of very thin skin with very small porosity. The membrane porosity develops

very rapidly through the depth suddenly in the direction of the membrane depth. No effect of solvent type, membranes formed from a low polymer concentration (i.e., 12 wt.%) were comprised of finger-like macro-voids with interconnections extended to the bottom of the membranes. However, the presence of PEG suppressed the formation of the finger-like macro-voids and created more spongy-like porous structures. Membranes with low porosity may be attributed to the increase in polymer concentrations and the delayed demixing, less finger-like pores, lower mean pore size, while there was a denser and thicker layer on the top.

3.3. Zeta potential of the membranes

The zeta potential values of the CA/PSPEG nanocomposites membranes as a function of pH are presented in Fig. 5. It was found that the CA/PSPEG nanocomposites membrane had a slightly negative surface charge. Practically, only 40%–50% of the primary hydroxyl groups on the cellulose surface were converted to acetyl during the acetylation reaction and therefore, some hydroxyl groups remained unreacted on the CA, contributing to the slightly

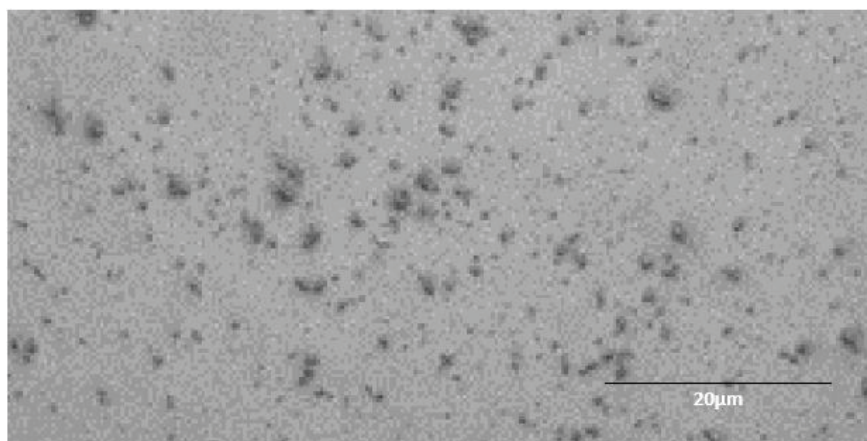


Fig. 4. Cross-sectional SEM images of modified CA/PSPEG membranes.

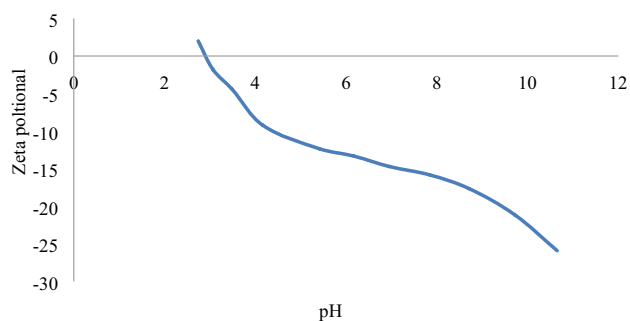


Fig. 5. Zeta potential values of the CA/PSPEG membranes.

low negative charge of the CA/PSPEG membrane [12]. The change in the zeta potential values of the CA/PSPEG membrane by varying the pH of the electrolyte was very minor, indicative of the low charge density of the pristine CA/PSPEG membrane. Furthermore, as the PEG content in the polymer matrix increased, the membrane possessed more negative surface charges.

3.4. Molecular weight cut-off determination of pressure filtration membranes

Through the study on the MWCO and the capacity of the UF CA/PSPEG composite membrane to remove the different partial weights from PEG (1,000–10,000) as shown in Fig. 6, it was noted that with the increase in the molecular weight, the membrane isolates with a higher capacity than the smaller weights. It was also observed that reservation in molecular weights higher than 4,000 reaches 85%–90% and up to 100% in weights higher than 6,000, where the PEG volume becomes large enough to be difficult to creep out of the prepared CA/PSPEG composite membrane. [27]. It appears from these results that the physicochemical properties of PES composite membranes under this study were quite similar in terms of their surface charge, surface topography, thickness, and nature (hydrophobicity/hydrophilicity) of surface and pores. However, these CA/PSPEG composite membranes were different according to their conductivity, porosity, and macropore distribution values, which increased with an increase in MWCO of PES membranes as reported in [9]. Furthermore, macropore distribution in the filtrating layer of such asymmetric membranes was directly related to the MWCO of PEG membranes.

3.5. Water permeability of membranes

The permeate flux of deionized water was measured at different temperatures with constant cross flow velocity (CFV) = 6 m s^{-1} to determine the water membrane permeability. The results of the pure water flux of CA/PSPEG

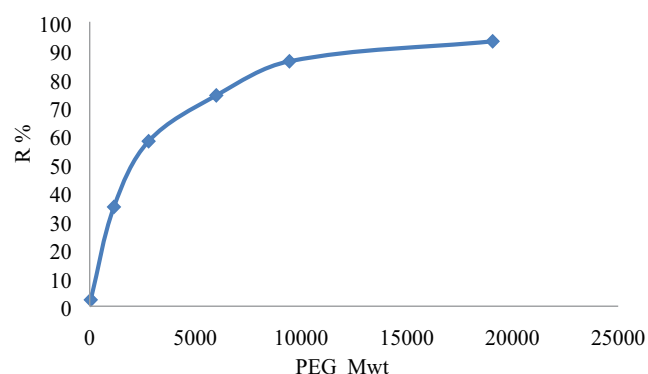


Fig. 6. MWCO curve for CA/PSPEG membranes using the PEG as solute filtration.

membranes are tabulated in Table 2. Increasing the amount of PEG to 0.1 wt.% led to an increase in the water flux of CA/PSPEG ($17 \text{ kg m}^{-2} \text{ h}^{-1}$) in comparison with the CA/PSPEG membrane. However, the flux of PES/CS₂ was still higher than that of the PES membrane. The addition of PEG to the waste polystyrene composite membrane shows enhancement in the permeability of the membrane to $2 \text{ kg m}^{-2} \text{ h}^{-1}$ [28,29].

The results obtained from the experiments with suspended kaolin water showed that the permeate flux increases from the beginning of the run to the steady-state condition and it was higher at the higher temperature (Fig. 7). In fact, as an example, for a fixed TMP of 10 bar, the permeate flux increased by 80.5% from its initial value when the operating temperature was set at 318 K. The increase in permeate flux as the temperature is a consequence of the of membrane fouling and concentration polarization under higher temperature. The temperature of suspended kaolin water was

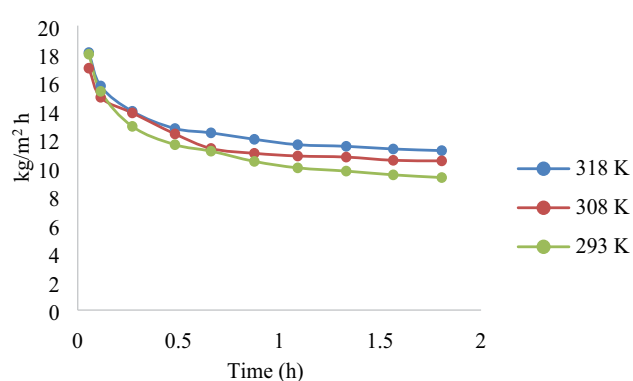


Fig. 7. Effect of temperature on permeate flux of CA/PSPEG composite membrane (CFV = 6 m s^{-1} and TMP = 10 bar).

Table 2
Water permeability and characteristics of membranes

Membrane	Pure water flux ($\text{kg m}^{-2} \text{ h}^{-1}$) (permeability ($\text{kg m}^{-2} \text{ h}^{-1} \text{ MPa}$))	Skin-layer thickness (μm)	Bulk porosity (%)	Water contact angle ($^\circ$)
CA/PSPEG	2	50	59 ± 2	7

controlled from 293 to 318 K using a water bath. Fig. 7 shows the variation of the permeate flux after 2 h of filtration at different feed temperatures. As seen in Fig. 7, at a higher temperature, cake layer formation is limited, and permeate flux is almost constant. It must be mentioned that by increasing temperature, permeate flux increases. The temperature has double effects on permeation flux; increasing temperature decreases viscosity, and as a result, increases permeation flux [30]. From another point of view, increasing temperature increases osmotic pressure and this decreases permeation flux. Therefore, the bilateral effects of temperature must be specified. Additionally, higher feed temperature leads to lower viscosity of feed and also higher solubility of some feed constituents. The same reduces concentration polarization and transport of solvent through the membrane intensifies, yielding a higher permeates flux.

3.6. Effect of pH

Fig. 8 displays the nephelometric turbidity units (NTU) and $R\%$ interaction and the change in pH of the solution during the filtration process at different pH 3.5 and 7.5. The membrane surface charge and the aggregate size formation during the UF treatment were controlled by the suspension pH for the organic pollutants in water [31,32]. The reported results recommend that the pH effect on the UF of organic compounds in polluted water is correlated to many factors. Firstly, the surface membrane ionization state. Secondly, the hydroxyl radicals formation by the ionic interaction of clay hydroxide ions and composite membrane surface. Thirdly, the clustering of kaolin particles [33]. The adsorption of the kaolin would be higher near the point of zero charges (pzc) of the composite membrane. In this study, the measured point of zero charges for the composite membrane was approximately 7.3. Therefore, the composite membrane charged positively in acidic conditions ($\text{pH} < 7.3$), whereas charged negatively under alkaline conditions ($\text{pH} > 6.3$). This favors the adsorption of positively charged contaminants [34,35] at $\text{pH} > \text{pzc}$ and adsorption of negatively charged contaminants at $\text{pH} < \text{pzc}$. It is worth mentioning that most clay minerals have negative charges. At low pH ($< \text{pzc}$), the adsorption of organic pollutants onto the composite membrane is improved [36]. At high pH ($> \text{pzc}$), OH^- is easily generated as more OH^- ions are available on the composite membrane surface and enhance the process efficiency. However, when $\text{pH} < 7.3$, composite membrane tends to cluster resulting in a reduction in the effective composite membrane surface area for photon capture and kaolin adsorption and filtration, which could deteriorate the UF rate [37,38].

3.7. Effect of sintering temperatures

Tian et al. [34] and Du et al. [35] investigated the performance of composite membrane in terms of water permeation and kaolin rejection to evaluate the effect of different sintering temperatures on the performance of the composite membrane, water permeation, and kaolin rejection tests. Fig. 9 shows the experimental results on water permeation of composite membrane that sintered at different sintering temperatures. The obtained results showed that the composite membrane sintered at 353 K has the lowest

water turbidity with a removal efficiency of 97.5%. These findings were influenced by the membrane densification and pore size shrinkage that occurred when the higher temperature was used, which observed previously from SEM images of the outer membrane surface of the composite membrane [39,40].

3.8. Effect of contact time on the filtration process

The membrane was first tested in dead-end cell mode with clay polluted water as a feed solution. In Fig. 10,

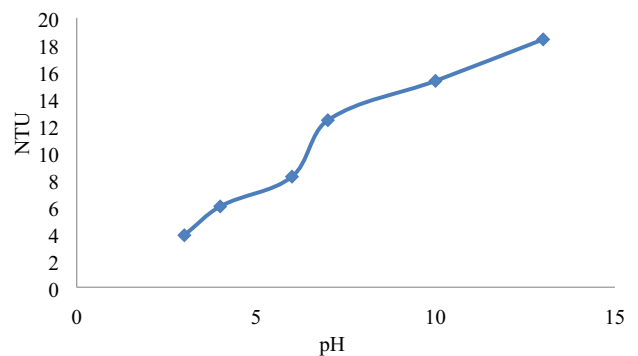


Fig. 8. The relation between pH and NTU for prepared composite membrane.

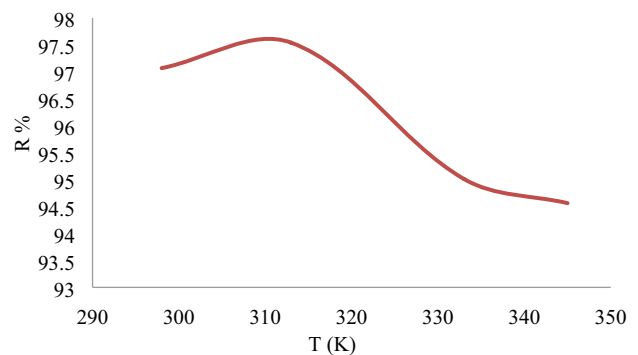


Fig. 9. Kaolinite rejection during filtration on CA/PSPEG composite membranes sintered at different temperatures.

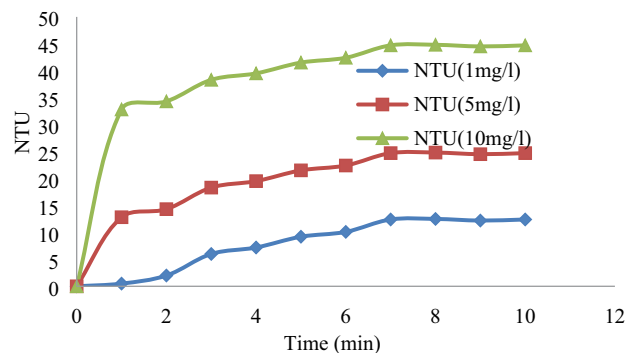


Fig. 10. CA/PSPEG composite membranes performance for ultra-filtration of kaolin suspensions.

the NTU as a function of experimental time has been shown. The membrane showed a stable NTU of 45 NTU after 6 min. [41]. It can be said that the CA/PSPEG membrane yielded an excellent treatment performance in terms of organic removal in the three phases with average values of 98.6% [42]. In terms of kaolinite removal, the system showed very good performance. This result could be related to the increased kaolinite loading rate that promoted an increase in heterotrophic activity [43]. The CA/PSPEG membrane achieved very high kaolinite removal in this study which is in good agreement with previous studies on similar plant configurations [44,45].

3.9. Influence of solution pH on membrane performance

3.9.1. pH effect on salts in binary solutions

The pH of the feed solution has a major effect on the membrane surface charge. This study mainly focused on membrane separation efficiency in the ionic species removal process. Hydrophilic behavior can be recognized by the hydrated polymer membrane surface, which resulted in controlling the sign and the charge density of the membrane surface by pH control. The point of zero charges (pzc) matches the pH when the surface charge is null (pHpzc). PZC is the value for the electric charges of the fixed cations globally neutralize anions [46]. At a pH > pzc, the acidic dissociation of the surface hydroxyl groups leads to a negative surface charge validated by the presence of HO⁻ groups. Whereas, the positive charge when the pH < pzc is deduced based on proton addition to the neutral aquo complex due to the presence of R-OH²⁺ groups [28]. Fig. 11 presents the effect of feed solution pH on salts rejection at an applied pressure of 6 bar and initial concentration of 7,192 mg L⁻¹. In the acidic pH range, the salt's rejection rise continued up to a maximum pH value of about 12. But, the rejection reduced with the pH in the neutral range.

The strong interactions developed between the divalent cations and the negatively charged membrane (pH < pzc) resulted in high cation rejection. The Na and Ca ions rejection also increased when the pH value increased due to electro-neutrality consideration, illustrated by a rejection rate which exceeded 80% for divalent cation Mg, and 50% for monovalent cation (Na and K). The ion separation is highly governed by the Donnan exclusion (charge effect) [47]. Aslam et al [48] elucidated this performance by the distribution variation on the membrane surface charge as

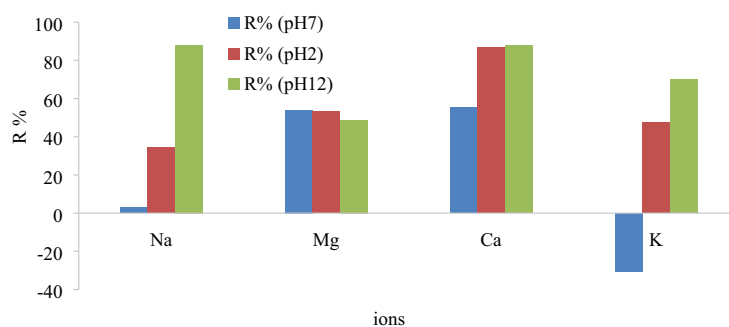


Fig. 11. Influence of feed pH on salts rejection (%) in binary solutions at $\Delta P = 6$ bar and $C_i = 7,192$ mg salts L⁻¹.

a function of pH. At pH_{pzc} the membrane is uncharged (no electrostatic repulsion), sieving mechanism based on ion size controls the selectivity [45]. For pH > pzc, as shown in Fig. 12, decrease in cations rejection occurred at pH = 7. This reduction in salt retention detected when the pH increased can be clarified by an increase in the positive charge of the membrane in the presence of the different electrolytes; which assists the cations passage through the membrane [46,47].

3.9.2. Influent pH effect on kaolinite filtration

Fig. 13 demonstrates the performance of the developed membrane in terms of rejection of kaolinite as suspension solids. The maximum operating pressure for the rejection experiments was 3 bar. The antifouling characteristic also decreases the efforts of membrane cleaning and declination of fluxes [49]. The higher rejection range and permeability results may be associated with the adsorption of water molecules in hydrophilic composite UF surfaces [13,50].

Fig. 8 demonstrates the kaolinite rejections as a function of concentrations and pH of the feed solution. Considering the same pH value (pH of 7.4–12), the rejection percentage increased with an increasing initial salt concentration of the feed solution with 49% rejection was observed. The rejection curves in Fig. 6 revealed a stable condition (running period of 100 min) and afterward, no significant changes were observed. However, the best kaolinite rejection was observed at 5 bar TMP promoting low-pressure filtration processes resulting in lower energy consumption [51,52].

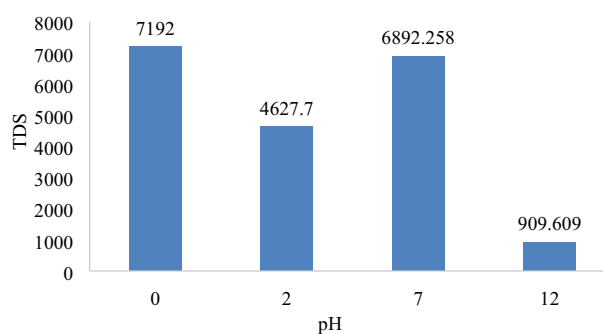


Fig. 12. Influent pH effect on total dissolved solids reduction at $\Delta P = 6$ bar and $C_i = 7,192$ mg salts L⁻¹.

3.9.3. Effect of pressure on the rejection of kaolinite through the membrane

Fig. 14 shows the kaolinite retention performance of composite membranes. For the film that was prepared with dense and small pore size, it is not easy for kaolinite to pass under 10 bar. In addition, the results indicated that the pure water presence of the hierarchical membranes increased with the increase in pressure. The ratio of the prepared membrane was 0.02 gave an encouraging efficiency with a pure water permeance of $95 \text{ kg m}^{-2} \text{ h}^{-1} \text{ MPa}^{-1}$ and a rejection ability 99%, corresponding to a stokes diameter of 4.46 nm. As seen in Fig. 14, the pure permeance of the composite membrane increased almost linearly as the operating pressure raised. This suggested that the membrane contained uniform inter-crystalline pores [53].

3.10. Effect of feed temperature on membrane

The decrease of the permeate flux s from the beginning of the run to the steady-state condition was lower at the higher temperature as shown in Fig. 3. In fact, as an example, for a fixed TMP of 4 bar, permeate flux decreased by 80.5% from its initial value when the operating temperature was set at 20°C. The small decrement in permeate flux as temperature increases is a result of membrane fouling reduction and concentration polarization under higher temperature [52].

Textile wastewater temperature was varied from 20°C to 40°C using a water bath. Fig. 15 displays the variation

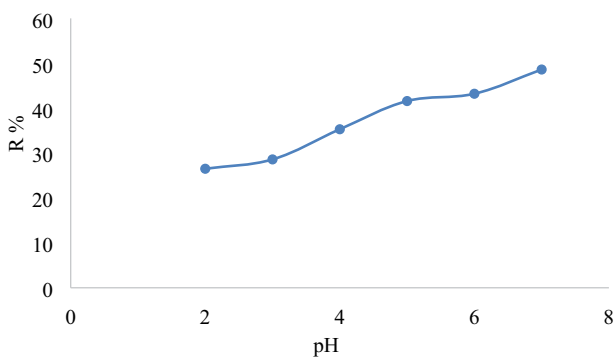


Fig. 13. Influent pH effect on kaolinite rejection (%) in solutions at $\Delta P = 6 \text{ bar}$ and $C_i = 100 \text{ mg salts L}^{-1}$.

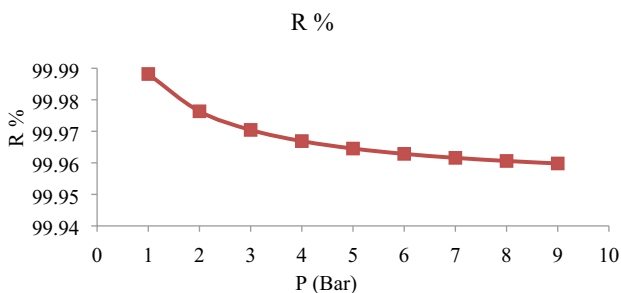


Fig. 14. Effect of TMP on rejection % at different temperatures for contaminated water.

of the permeate flux after 6 h of filtration at different feed temperatures. The permeate flux increases by 18% with increases in feed temperature from 20°C to 40°C. As viewed, at a higher temperature cake layer formation is limited, and permeate flux is almost constant [54,55]. Alike, concentration polarization and transport of solvent through the membrane intensifies have been reduced, yielding a higher permeates flux. When the feed temperature increases, it normally surges the energy cost and the scaling potential and diminishes the membrane durability system despite superior stability of ceramic membrane compared to the polymeric membrane in thermal condition [56].

3.11. Effect of recovery change on the flux and rejection

The water recovery rate was studied as a function of R and flux as shown in Fig. 13. Yet, it is possible to increase the water recovery efficiency by increasing the amount of the polluted water fed across the membrane as shown; with increasing the relative recoveries for salts and kaolinite, the flux will be higher compared with the rejection. No significant variations were found in the results of the study duration [57]. The overall treated water recoveries have been studied for all cases by dividing the amount of treated water extracted via the membranes by the total amount of polluted water-fed (Fig. 16). Especially when moving towards large-scale production of pure water via the composite membrane, the overall recovery should be high to ensure high reaction rates and sufficient salts and kaolinite

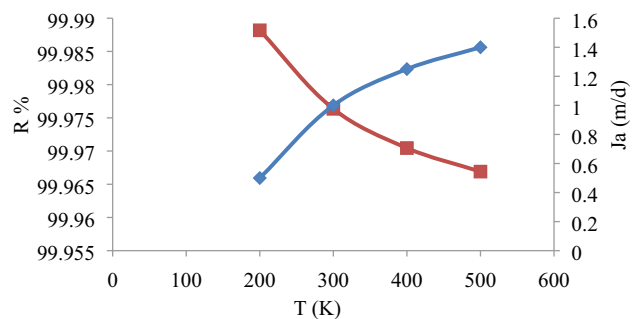


Fig. 15. Effect of temperature on permeate flux ($\text{CFV} = 6 \text{ m s}^{-1}$ and $\text{TMP} = 2.05 \text{ bar}$).

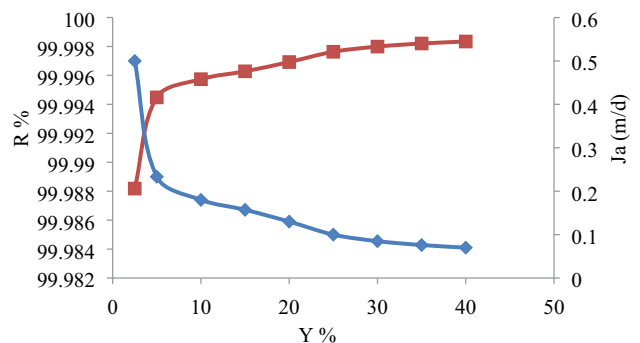


Fig. 16. Result of power output and water recovery rate with sweep air amount fed to the membrane.

extraction. The overall recoveries do not tell the full story on the composite membrane performance [13,58].

4. Conclusion

The use of CA/PSPEGUF membrane in kaolinite removal from prepared solutions and commercial mineral water was the main concept in this research. Factors such as pH, applied temperature, initial concentration of kaolinite were examined to estimate the CA/PSPEG membrane efficiency. The CA/PSPEG membrane selection strictly relied on influent pH which changed the membrane charge (amphoteric character: positive in acid medium and negative in basic medium). The high rejection of kaolinite was obtained around pH_{pzc} and thus varying the CA/PSPEG membrane performance.

The reduction of membrane fouling by grafting and combination with PS pretreatment can be a viable option to improve the ceramic membrane filtration performance. Larger aggregates (1–0.4 μm) appeared to generate a significantly lower membrane fouling rate. Considering the operation cost, the optimum conditions appear to be a pH of 7 with an NTU of 10 at temperature 310 K with equilibrium time 10 min and maximum flux 2.5 m d^{-1} at recovery 40% from feed water.

Finally, the CA/PSPEGUF membrane is considered as an alternative treatment process for filtration of clay, sand, and organics contaminated water. The better performance of the CA/PSPEG was due to the hollow fiber membrane, which acted as a solid–liquid separator and thereby enabled the filtration process in water treatment to maintain a high microalgae concentration to obtain a high amount of suspended solids removal, in addition, to eradicating suspended solids and microorganisms inhibitory effects.

References

- [1] N. Nagaraja, L. Skillman, Z.W. Xie, S. Jiang, G. Ho, D. Li, Investigation of compounds that degrade biofilm polysaccharides on reverse osmosis membranes from a full scale desalination plant to alleviate biofouling, *Desalination*, 403 (2017) 88–96.
- [2] S.J. Meng, Y. Liu, Transparent exopolymer particles (TEP)-associated membrane fouling at different Na^+ concentrations, *Water Res.*, 111 (2017) 52–58.
- [3] H.J. Oh, J.E. McGrath, D.R. Paul, Kinetics of poly(ethylene glycol) extraction into water from plasticized disulfonated poly(arylene ether sulfone) desalination membranes prepared by solvent-free melt processing, *J. Membr. Sci.*, 524 (2017) 257–265.
- [4] J. Zuo, T.-S. Chung, G.S. O'Brien, W. Kosar, Hydrophobic/hydrophilic PVDF/Ultem® dual-layer hollow fiber membranes with enhanced mechanical properties for vacuum membrane distillation, *J. Membr. Sci.*, 523 (2017) 103–110.
- [5] O.R. Lokare, S. Tavakkoli, S. Wadekar, V. Khanna, R.D. Vidic, Fouling in direct contact membrane distillation of produced water from unconventional gas extraction, *J. Membr. Sci.*, 524 (2017) 493–501.
- [6] L. Luo, T.-S. Chung, M. Weber, C. Staudt, C. Maletzko, Molecular interaction between acidic sPPSU and basic HPEI polymers and its effects on membrane formation for ultrafiltration, *J. Membr. Sci.*, 524 (2017) 33–42.
- [7] B. Zhu, X.R. Hu, J.-W. Shin, I.-S. Moon, Y. Muraki, G. Morris, S. Gray, M. Duke, A method for defect repair of MFI-type zeolite membranes by multivalent ion infiltration, *Microporous Mesoporous Mater.*, 237 (2017) 140–150.
- [8] S.G. Lim, M.J. Park, S. Phuntsho, L.D. Tijing, G.M. Nisola, W.-G. Shim, W.-J. Chung, H.K. Shon, Dual-layered nano-composite substrate membrane based on polysulfone/graphene oxide for mitigating internal concentration polarization in forward osmosis, *Polymer*, 110 (2017) 36–48.
- [9] H.-Z. Zhang, Z.-L. Xu, Y.-J. Tang, H. Ding, Highly chlorine-tolerant performance of three-channel capillary nanofiltration membrane with inner skin layer, *J. Membr. Sci.*, 527 (2017) 111–120.
- [10] M. Fathy, Th.A. Moghny, M.A. Mousa, A.-H.A.-A. El-Bellihi, A.E. Awadallah, Sulfonated ion exchange polystyrene composite resin for calcium hardness removal, *Int. J. Emerging Technol. Adv. Eng.*, 5 (2015) 20–29.
- [11] M. Fathy, Th.A. Moghny, A.E. Awadallah, A.-H.A.-A. El-Bellihi, Study the adsorption of sulfates by high cross-linked polystyrene divinylbenzene anion-exchange resin, *Appl. Water Sci.*, 7 (2017) 309–313.
- [12] S. Zhao, Z. Wang, A loose nano-filtration membrane prepared by coating HPAN UF membrane with modified PEI for dye reuse and desalination, *J. Membr. Sci.*, 524 (2017) 214–224.
- [13] H.S. Kandeel, N.A. Badawya, A.A. Hamada, M. El-Sayed, M. Fathy, A.A.G. Al-Gamal, T.A. Moghny, Desalination aspects of PSSA-g-PEG copolymer and its graphene composite membranes, *Int. J. Chem. Sci.*, 16 (2018) 1–13.
- [14] S.S. Manickam, G.Z. Ramon, J.R. McCutcheon, Modeling the effect of film-pore coupled transport on composite forward osmosis membrane performance, *J. Membr. Sci.*, 523 (2017) 533–541.
- [15] J.F. Zheng, M. Li, K. Yu, J.H. Hu, X. Zhang, L.J. Wang, Sulfonated multiwall carbon nanotubes assisted thin-film nanocomposite membrane with enhanced water flux and anti-fouling property, *J. Membr. Sci.*, 524 (2017) 344–353.
- [16] R. Hosny, M. Fathy, M. Ramzi, Th.A. Moghny, S.E.M. Desouky, S.A. Shama, Treatment of the oily produced water (OPW) using coagulant mixtures, *Egypt. J. Pet.*, 25 (2016) 391–396.
- [17] M. Yang, C.W. Zhao, S.F. Zhang, P. Li, D.Y. Hou, Preparation of graphene oxide modified poly(m-phenylene isophthalamide) nanofiltration membrane with improved water flux and antifouling property, *Appl. Surf. Sci.*, 394 (2017) 149–159.
- [18] M. Yasukawa, S. Mishima, Y. Tanaka, T. Takahashi, H. Matsuyama, Thin-film composite forward osmosis membrane with high water flux and high pressure resistance using a thicker void-free polyketone porous support, *Desalination*, 402 (2017) 1–9.
- [19] R.E. da Costa, M.A. Lobo-Recio, A.A. Battistelli, J.P. Bassin, T.J. Belli, F.R. Lapolli, Comparative study on treatment performance, membrane fouling, and microbial community profile between conventional and hybrid sequencing batch membrane bioreactors for municipal wastewater treatment, *Environ. Sci. Pollut. Res.*, 25 (2018) 32767–32782.
- [20] H. Yang, M. Elma, D.K. Wang, J. Motuzas, J.C. Diniz da Costa, Interlayer-free hybrid carbon-silica membranes for processing brackish to brine salt solutions by pervaporation, *J. Membr. Sci.*, 523 (2017) 197–204.
- [21] L. Li, K.K. Sirkar, Studies in vacuum membrane distillation with flat membranes, *J. Membr. Sci.*, 523 (2017) 225–234.
- [22] L. Keulen, L.V. van der Ham, N.J.M. Kuipers, J.H. Hanemaaijer, T.J.H. Vlught, S. Kjelstrup, Membrane distillation against a pressure difference, *J. Membr. Sci.*, 524 (2017) 151–162.
- [23] M. Larronde-Larrette, X. Jin, Microalgal biomass dewatering using forward osmosis membrane: influence of microalgae species and carbohydrates composition, *Algal Res.*, 23 (2017) 12–19.
- [24] O. Labban, C. Liu, T.H. Chong, J.H. Lienhard V, Fundamentals of low-pressure nanofiltration: membrane characterization, modeling, and understanding the multi-ionic interactions in water softening, *J. Membr. Sci.*, 521 (2017) 18–32.
- [25] J. Lee, S.Y. Jeong, Y. Ye, V. Chen, S. Vigneswaran, T. Leiknes, Z.W. Liu, Protein fouling in carbon nanotubes enhanced ultrafiltration membrane: fouling mechanism as a function of pH and ionic strength, *Sep. Purif. Technol.*, 176 (2017) 323–334.
- [26] O.S. Kushwaha, C. Ver Avadhani, N.S. Tomer, R.P. Singh, Accelerated degradation study of highly resistant polymer

- membranes for energy and environment applications, *Adv. Chem. Sci.*, 3 (2014) 19–30.
- [27] Y. Bagbi, A. Pandey, P.R. Solanki, Chapter 10 – Electrospun Nanofibrous Filtration Membranes for Heavy Metals and Dye Removal, S. Thomas, D. Pasquini, S.-Y. Leu, D.A. Gopakumar, Eds., *Nanoscale Materials in Water Purification: A Volume in Micro and Nano Technologies*, Elsevier, 2019, pp. 275–288 Available at: <https://www.elsevier.com/books/book-series/micro-and-nano-technologies>.
- [28] N. Ghaemi, P. Daraei, F.S. Akhlaghi, Polyethersulfone nanofiltration membrane embedded by chitosan nanoparticles: fabrication, characterization and performance in nitrate removal from water, *Carbohydr. Polym.*, 191 (2018) 142–151.
- [29] M. Fujiwara, Water desalination using visible light by disperse red 1 modified PTFE membrane, *Desalination*, 404 (2017) 79–86.
- [30] R. Lafi, L. Gzara, R.H. Lajimi, A. Hafiane, Treatment of textile wastewater by a hybrid ultrafiltration/electrodialysis process, *Chem. Eng. Process. Process Intensif.*, 132 (2018) 105–113.
- [31] Y.C. Woo, L.D. Tijing, M.J. Park, M.W. Yao, J.-S. Choi, S. Lee, S.-H. Kim, K.-J. An, H.K. Shon, Electrospun dual-layer nonwoven membrane for desalination by air gap membrane distillation, *Desalination*, 403 (2017) 187–198.
- [32] D. Ferrando, C. Ziemba, M. Herzberg, Revisiting interrelated effects of extracellular polysaccharides during biofouling of reverse osmosis membranes: viscoelastic properties and biofilm enhanced osmotic pressure, *J. Membr. Sci.*, 523 (2017) 394–401.
- [33] S.N. Wang, D.K. Wang, S. Smart, J.C. Diniz da Costa, Improved stability of ethyl silicate interlayer-free membranes by the rapid thermal processing (RTP) for desalination, *Desalination*, 402 (2017) 25–32.
- [34] M. Tian, Y.-N. Wang, R. Wang, A.G. Fane, Synthesis and characterization of thin film nanocomposite forward osmosis membranes supported by silica nanoparticle incorporated nanofibrous substrate, *Desalination*, 401 (2017) 142–150.
- [35] X. Du, G.Y. Liu, F.S. Qu, K. Li, S. Shao, G.B. Li, H. Liang, Removal of iron, manganese and ammonia from groundwater using a PAC-MBR system: the anti-pollution ability, microbial population and membrane fouling, *Desalination*, 403 (2017) 97–106.
- [36] T.E. Thomas, S.A. Aani, D.L. Oatley-Radcliffe, P.M. Williams, N. Hilal, Laser Doppler Electrophoresis and electro-osmotic flow mapping: A novel methodology for the determination of membrane surface zeta potential, *J. Membr. Sci.*, 523 (2017) 524–532.
- [37] H.A. Maddah, A.S. Alzhrani, M. Bassyouni, M.H. Abdel-Aziz, M. Zoromba, A.M. Almalki, Evaluation of various membrane filtration modules for the treatment of seawater, *Appl. Water Sci.*, 8 (2018) 150.
- [38] W. Falath, A. Sabir, K.I. Jacob, Novel reverse osmosis membranes composed of modified PVA/Gum Arabic conjugates: biofouling mitigation and chlorine resistance enhancement, *Carbohydr. Polym.*, 155 (2017) 28–39.
- [39] S. Shanmuganathan, P. Loganathan, C. Kazner, M.A.H. Johir, S. Vigneswaran, Submerged membrane filtration adsorption hybrid system for the removal of organic micropollutants from a water reclamation plant reverse osmosis concentrate, *Desalination*, 401 (2017) 134–141.
- [40] J. Deshpande, K. Nithyanandam, R. Pitchumani, Analysis and design of direct contact membrane distillation, *J. Membr. Sci.*, 523 (2017) 301–316.
- [41] D.W. Lee, Y. Lee, S.S. Choi, S.-H. Lee, K.-W. Kim, Y.H. Lee, Effect of membrane property and feed water organic matter quality on long-term performance of the gravity-driven membrane filtration process, *Environ. Sci. Pollut. Res.*, 26 (2019) 1152–1162.
- [42] S.-J. Park, W. Choi, S.-E. Nam, S.W. Hong, J.S. Lee, J.-H. Lee, Fabrication of polyamide thin film composite reverse osmosis membranes *via* support-free interfacial polymerization, *J. Membr. Sci.*, 526 (2017) 52–59.
- [43] W. Choi, K.-Y. Chun, J.W. Kim, C.-S. Han, Ion transport through thermally reduced and mechanically stretched graphene oxide membrane, *Carbon*, 114 (2017) 377–382.
- [44] Z.Z. Zhu, X. Luo, F.F. Yin, S.Y. Li, J.R. He, Clarification of *Jerusalem Artichoke* extract using ultra-filtration: effect of membrane pore size and operation conditions, *Food Bioprocess Technol.*, 11 (2018) 864–873.
- [45] Q. Chen, Y.-Y. Du, K.-M. Li, H.-F. Xiao, W. Wang, W.-M. Zhang, Graphene enhances the proton selectivity of porous membrane in vanadium flow batteries, *Mater. Des.*, 113 (2017) 149–156.
- [46] G. Chen, R.X. Liu, H.K. Shon, Y.Q. Wang, J.F. Song, X.-M. Li, T. He, Open porous hydrophilic supported thin-film composite forward osmosis membrane via co-casting for treatment of high-salinity wastewater, *Desalination*, 405 (2017) 76–84.
- [47] M.I. Baig, P.G. Ingole, W.K. Choi, J.-d. Jeon, B.Y. Jang, J.H. Moon, H.K. Lee, Synthesis and characterization of thin film nanocomposite membranes incorporated with surface functionalized silicon nanoparticles for improved water vapor permeation performance, *Chem. Eng. J.*, 308 (2017) 27–39.
- [48] M. Aslam, A. Charfi, G. Lesage, M. Heran, J.W. Kim, Membrane bioreactors for wastewater treatment: a review of mechanical cleaning by scouring agents to control membrane fouling, *Chem. Eng. J.*, 307 (2017) 897–913.
- [49] G. Amy, N. Ghaffour, Z.Y. Li, L. Francis, R.V. Linares, T. Missimer, S. Lattemann, Membrane-based seawater desalination: present and future prospects, *Desalination*, 401 (2017) 16–21.
- [50] P. Roy Choudhury, S. Majumdar, S. Sarkar, B. Kundu, G.C. Sahoo, Performance investigation of Pb(II) removal by synthesized hydroxyapatite based ceramic ultrafiltration membrane: bench scale study, *Chem. Eng. J.*, 355 (2019) 510–519.
- [51] S.J. Yang, Q.F. Zou, T.H. Wang, L.P. Zhang, Effects of GO and MOF@GO on the permeation and antifouling properties of cellulose acetate ultrafiltration membrane, *J. Membr. Sci.*, 569 (2019) 48–59.
- [52] A. Al-Jubainawi, Z.J. Ma, Y. Guo, L.D. Nghiem, P. Cooper, W.H. Li, Factors governing mass transfer during membrane electrodialysis regeneration of LiCl solution for liquid desiccant dehumidification systems, *Sustainable Cities Soc.*, 28 (2017) 30–41.
- [53] L. Peng, X.H. Xu, X. Yao, H. Liu, X.H. Gu, Fabrication of novel hierarchical ZSM-5 zeolite membranes with tunable mesopores for ultrafiltration, *J. Membr. Sci.*, 549 (2018) 446–455.
- [54] M. Alberto, J.M. Luque-Alled, L. Gao, M. Iliut, E. Prestat, L. Newman, S.J. Haigh, A. Vijayaraghavan, P.M. Budd, P. Gorgojo, Enhanced organophilic separations with mixed matrix membranes of polymers of intrinsic microporosity and graphene-like fillers, *J. Membr. Sci.*, 526 (2017) 437–449.
- [55] A.L. Ahmad, A.A. Abdulkarim, Z.M.H. Mohd Shafie, B.S. Ooi, Fouling evaluation of PES/ZnO mixed matrix hollow fiber membrane, *Desalination*, 403 (2017) 53–63.
- [56] A. Alkudhiri, N. Hilal, Air gap membrane distillation: a detailed study of high saline solution, *Desalination*, 403 (2017) 179–186.
- [57] J. Adams, N. Bighane, W.J. Koros, Pore morphology and temperature dependence of gas transport properties of silica membranes derived from oxidative thermolysis of polydimethylsiloxane, *J. Membr. Sci.*, 524 (2017) 585–595.
- [58] F.E. Ahmed, B.S. Lalia, N. Hilal, R. Hashaikeh, Electrically conducting nanofiltration membranes based on networked cellulose and carbon nanostructures, *Desalination*, 406 (2017) 60–66.